Complexation of Np(V) with the Dicarboxylates, Malonate, and Succinate: Complex Stoichiometry, Thermodynamic Data, and Structural Information

Martin M. Maiwald, Katharina Müller, Karsten Heim, Jörg Rothe, Kathy Dardenne, André Rossberg, Carsten Koke, Michael Trumm, Andrej Skerencak-Frech,* and Petra J. Panak

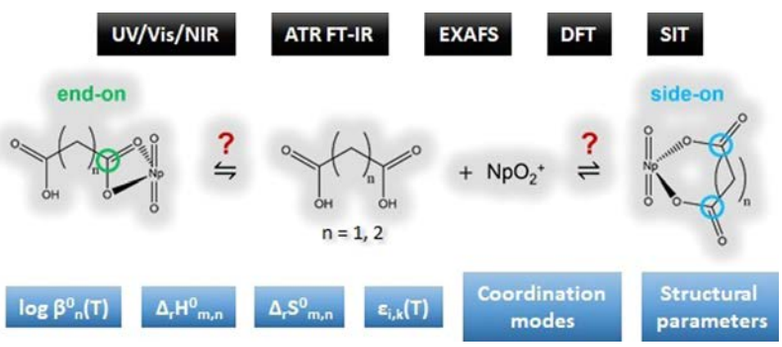

ABSTRACT: The complexation of Np(V) with malonate and succinate is studied by different spectroscopic techniques, namely, attenuated total reflection Fourier transform infrared (ATR FT IR) and extended X ray absorption fine structure (EXAFS) spectroscopy, as well as by quantum chemistry to determine the speciation, thermodynamic data, and structural information of the formed complexes. For complex stoichiometries and the thermodynamic functions (log $\beta_n^\circ(\Theta)$, $\Delta_r H_n^\circ$, $\Delta_r S_n^\circ$), near infrared absorption spectroscopy (vis/NIR) is applied. The complexation reactions are investigated as a function of the total concentration of malonate ($[Mal^{2-}]_{total}$) and succinate ($[Succ^{2-}]_{total}$), ionic strength [I_m = 0.5−4.0 mol kg^{-1} $Na^+(Cl^-/ClO_4^-)$], and temperature (Θ = 20−85 °C). Besides the solvated NpO_2^+ ion, the formation of two Np(V) species with the stoichiometry $NpO_2(L)_n^{1-2n}$ (n = 1, 2, L = Mal^{2-}, $Succ^{2-}$) is observed. With increasing temperature, the molar fractions of both complex species increase and the temperature dependent conditional stability constants log $\beta_n'(\Theta)$ at given ionic strengths are determined by the law of mass action. The log $\beta_n'(\Theta)$ are extrapolated to IUPAC reference state conditions (I_m = 0) according to the specific ion interaction theory (SIT), revealing thermodynamic log $\beta_n^\circ(\Theta)$ values. For all formed complexes, [$NpO_2(Mal)^-$: log β_1°(25 °C) = 3.36 ± 0.11, $NpO_2(Mal)_2^{3-}$: log β_2°(25 °C) = 3.95 ± 0.19, $NpO_2(Succ)^-$: log β_1°(25 °C) = 2.05 ± 0.45, $NpO_2(Succ)_2^{3-}$: log β_2°(25 °C) = 0.75 ± 1.22], an increase of the stability constants with increasing temperature was observed. This confirmed an endothermic complexation reaction. The temperature dependence of the log $\beta_n^\circ(T)$ values is described by the integrated Van't Hoff equation, and the standard reaction enthalpies and entropies for the complexation reactions are determined. Furthermore, the sum of the specific binary ion−ion interaction coefficients $\Delta\varepsilon n^\circ(\Theta)$ for the complexation reactions are obtained as a function of the t from the respective SIT modeling as a function of the temperature. In addition to the thermodynamic data, the structures of the complexes and the coordination modes of malonate and succinate are investigated using EXAFS spectroscopy, ATR FT IR spectroscopy, and quantum chemical calculations. The results show that in the case of malonate, six membered chelate complexes are formed, whereas for succinate, seven membered rings form. The latter ones are energetically unfavorable due to the limited space in the equatorial plane of the Np(V) ion (as NpO_2^+ cation).

1. INTRODUCTION

As the long term radiotoxicity of spent nuclear fuel is determined by radionuclides with very long half life, the geochemical behavior of actinide elements (i.e., Np, Pu, and Am) is of particular interest in terms of nuclear waste disposal. The final emplacement of high level nuclear waste in deep geological formations is the most preferred disposal option.[1−3] The intrusion of water into a nuclear waste repository is an

important scenario which has to be considered for the safety case. Upon contact of the actinides with dissolved organic or inorganic ligands their (geo)chemical properties and migration behavior can strongly be affected.[1,4−19] In terms of nuclear waste disposal, it is a key step to obtain a profound knowledge of the aqueous (geo)chemistry of the actinides including the most relevant interaction mechanisms, which is based on reliable thermodynamic data like standard stability constants $\log \beta^\circ(\Theta)$, standard enthalpies $\Delta_r H_m^\circ$, and entropies $\Delta_R S_m^\circ$ of the reaction.

Independent of the host rock of the nuclear waste disposal, cementitious materials will be used for the construction of the geoengineered barriers. Organic additives [plasticizer/super plasticizers (SP)] are added to the concrete mixture in order to enhance the physical properties of the resulting cement and concrete. Regarding the interaction of SP with actinides, polycarboxylate−ether based macromolecules are of particular importance.[20−22] Due to their complex structure, the characterization of their complexation properties toward actinide ions is challenging. In addition, the decomposition of macromolecular organic molecules may lead to the formation of various smaller carboxylic ligands with different structures, which can also be released from the cementitious materials. Thus, small carboxylic compounds (e.g., oxalate, malonate, succinate, salicylate, and phthalate) may be used as reference systems for organic macromolecules and the respective degradation products to study the complexation properties of polycarboxylate ligands with actinides.

In the last few years, the complexation properties of trivalent actinides [An(III)) and lanthanides (Ln(III)] with model systems like oxalate, malonate, or succinate and with commercially available super plasticizers have been studied extensively.[23−27] However, thermodynamic data for pentava lent actinides ($An^VO_2^+$) are scarce.

In the present work, the formation and structure of Np(V) malonate and succinate complexes are studied and compared with the data for Np(V) oxalate complexes. These ligand systems are the simplest dicarboxylic ligands with terminal COO^- groups and an increasing C atom backbone from C_2−C_4. This allows the characterization of steric effects and the effect of multiple functional groups on the complex stability, the thermodynamic behavior and the structure of $An^VO_2^+$ complexes with organic ligands.

2. EXPERIMENTAL SECTION

Caution! ^{237}Np is a radioactive α emitter and must be handled with care in laboratories appropriate for handling transuranic elements. Radiation exposure or incorporation causes health risks!

The molal concentration scale (mol kg^{-1} H_2O^{-1} = mol kg^{-1}) was used for the preparation of the solutions in order to avoid changes of the concentration due to changes of the temperature or ionic strength. All chemicals, apart from Np(V), were purchased from Merck Millipore or Alfa Aesar and of reagent grade or higher purity. All solutions and samples were prepared with ultrapure water (Milli Q academic, Millipore, 18.3 MΩ cm).

2.1. Sample Preparation. For absorption spectroscopic measure ments the total initial Np(V) concentration $[NpO_2^+]_{total}$ was set to 2.5 × 10^{-4} mol kg^{-1} in H_2O by a dilution of 6.1 × 10^{-2} mol kg^{-1} $^{237}Np(V)$ stock solution with 3.47 × 10^{-3} mol kg^{-1} $HClO_4$. The oxidation state of the Np ion was adjusted electrochemically. Details on the preparation of the stock solution are given in the literature.[28] In all Np(V) sample solutions, the total proton concentration $[H^+]_{total}$ was adjusted to 4.9 × 10^{-5} mol kg^{-1} with a standardized 0.02 mol kg^{-1} $HClO_4$ (Merck, Titripur). For determination of the complex stoichiometry, the complexation of Np(V) with malonate (Mal^{2-}) and succinate ($Succ^{2-}$) was studied at a fixed ionic strength (I_m = 1.0 mol kg^{-1}) as a function of the total ligand concentration $[Mal^{2-}]_{total}$ = 0−7.0 × 10^{-2} mol kg^{-1}; $[Succ^{2-}]_{total}$ = 0−8.1 × 10^{-2} mol kg^{-1}); and temperature (Θ = 20−85 °C). The ligand concentrations were increased by the successive addition of portions of 0.34 mol kg^{-1} Na_2Mal solution (Sigma Aldrich, bioXtra) and respective Na_2Succ solution (Merck, for synthesis). The effect of the ionic strength and background electrolyte on the complexation is studied in NaCl and $NaClO_4$ media. The concentration of the background electrolytes was varied between $[NaCl]_{total}$ = 0.5−4.3 mol kg^{-1} and $[NaClO_4]_{total}$ = 0.5−2.4 mol kg^{-1} at fixed ligand concentrations ($[Mal^{2-}]_{total}$ = 2.1 × 10^{-3} mol kg^{-1}, 2.3 × 10^{-2} mol kg^{-1} and ($[Succ^{2-}]_{total}$ = 1.1 × 10^{-1} mol kg^{-1}, 1.6 × 10^{-1} mol kg^{-1}). The concentration of $NaClO_4$ was increased by successive titration with aqueous 14.1 mol kg^{-1} $NaClO_4$ solution (Merck, 99.99%). The amount of NaCl was increased by the addition of solid NaCl (Merck, Suprapur) to the samples. All chemicals were used without further purification. The total proton concentration in all titration solutions was equal to that of the Np(V) samples. The total concentrations are defined as $[H^+]_{total} = [H^+]_{eq} + [HL^-]_{eq} + 2 \times [H_2L]_{eq}$ and $[L^{2-}]_{total} = [L^{2-}]_{eq} + [HL^-]_{eq} + [H_2L]_{eq} + [NaL^-]_{eq}$ (L = Mal, Succ).

2.2. Vis/NIR Absorption Spectroscopy. The complexation of Np(V) with malonate and succinate in aqueous solution was studied by vis/NIR absorption spectroscopy between 20 and 85 °C. A Varian Cary 5G UV/Vis/NIR spectrophotometer in combination with a Lauda Eco E100 thermostatic system to control the temperature of the sample holder was used. The cuvettes (quartz glass, 1 cm path length, Hellma Analytics) were conditioned for 15 min at each temperature (10 °C step size) in a custom made copper sample holder before measurement to ensure chemical equilibrium. The spectra were recorded between 950 and 1050 nm with a data interval of 0.1 nm, a scan rate of 60 nm min^{-1} (average accumulation time 0.1 s), and a slit width of 0.7 nm in the double beam mode. For baseline correction, identical samples without Np(V) were measured.

2.3. Attenuated Total Reflection-Fourier Transform Infrared Spectroscopy. A Bruker Vertex 80/v vacuum spectrometer equipped with a mercury cadmium telluride detector was used for FT IR measurements. The spectra were recorded between 4000 and 600 cm^{-1} with a spectral resolution of 4 cm^{-1}. The attenuated total reflection (ATR) unit (DuraSamplIR II, Smiths Inc.) is a horizontal diamond crystal with nine internal reflections on the upper surface and an angle of incidence of 45°. A 200 μL flow cell was used to ensure adequate background subtraction without external thermal interference. The measurements were based on the principle of reaction induced infrared difference spectroscopy. Further exper imental details are given elsewhere.[29]

In situ ATR Fourier transform infrared (FT IR) spectroscopic measurements of the formed NpO_2^+ malonate and succinate complexes were performed in D_2O (Sigma Aldrich, 99.9 atom % D). This is due to the characteristic vibrational modes of the NpO_2^+ ion in solution that are generally detected below 850 cm^{-1} where strong interferences with modes of the bulk water (H_2O) occur.[30] All samples were prepared under an inert gas atmosphere (N_2) to reduce the content of H_2O. The total NpO_2^+ concentration was 2.0 × 10^{-3} mol kg^{-1} (malonate) or 1.0 × 10^{-3} mol kg^{-1} (succinate). The ionic strength was I_m = 1.0 mol kg^{-1} (Na^+, Mal^{2-}/$Succ^{2-}$/Cl^-). NaCl was used as a background electrolyte as it does not absorb light in the infrared region of interest. The total concentrations of malonate and succinate were $[Mal^{2-}/Succ^{2-}]_{tot}$ = 1.0 × 10^{-1} mol kg^{-1}. The pD_c was adjusted between 4.0 and 7.4 by the addition of small aliquots of 0.2 or 2 mol L^{-1} DCl and 0.2 mol L^{-1} NaOD. The respective acids and bases were prepared by diluting 35 wt % DCl (Sigma Aldrich, 35 wt % in D_2O, ≥ 99 atom % D) and 40 wt % NaOD (Alfa Aesar, 40 wt % in D_2O, 99.5 atom % D) with D_2O. The pD_c values were corrected according to pD = pH + 0.4.[31] Details on the definition of the conditional pH_c/pD_c values are given in the literature.[32,33] The NpO_2^+ concentration and the species distribution of the samples were confirmed after preparation by vis/NIR spectroscopy using a Varian Cary 5G spectrometer connected directly to the N_2 glovebox via optical fibers.

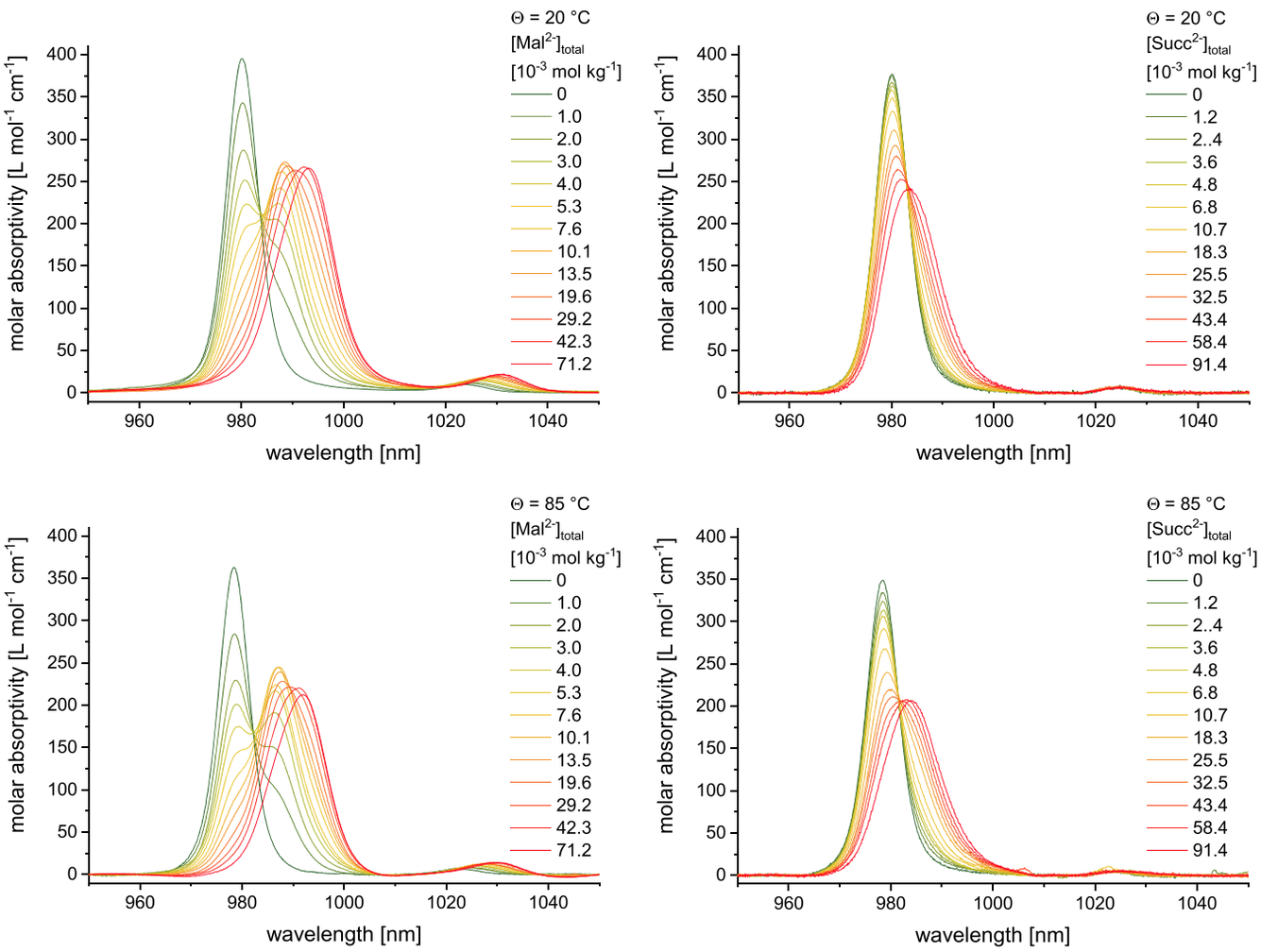

Figure 1. Absorption spectra of Np(V) with increasing malonate (left) and succinate (right) concentrations at Θ = 20 (top) and 85 °C (bottom) and I_m(NaClO4) = 1.0 mol kg^{-1}.

2.4. EXAFS Measurements. The Np L_3 edge EXAFS measurements were performed at an INE Beamline of the Karlsruhe Research Accelerator, KARA, at the Karlsruhe Institute of Technology (KIT), and the Rossendorf Beamline (ROBL) at the European Synchrotron Radiation Facility (ESRF) in Grenoble.[34−38] All EXAFS spectra were recorded in the fluorescence mode at 90° to the incident beam. At the INE Beamline, a 4 element Si SDD Vortex (SIINT) fluorescence and a 1 element Si Vortex 60EX SDD (SIINT) fluorescence detector were used. The ROBL Beamline was equipped with a 13 element Ge detector (Canberra). Details on the technical equipment and optical components of the beamlines are given in the literature.[34−38] Both beamlines were equipped with a double crystal monochromator detuning the peak flux intensity in the middle of the scan range to 70%. Within the EXAFS range, the measurements were performed at equidistant k steps. The integration time was increased with a $\sqrt{2}$ progression. The data were evaluated with the software packages EXAFSPAK, Athena Demeter 0.9.26, and Artemis Ifeffit 0.8.012.[39−41] Crystal structures of UO_2 malonate and UO_2 succinate were used for the calculation of the theoretical scattering phases and amplitudes using FEFF8.40 and replacing U by Np.[42−45] The k^2 and k^3 weighted raw EXAFS spectra were used for data evaluation.

2.5. Quantum Chemical Calculations. Structure optimizations of the Np(V) malonate and succinate complexes were performed on the density functional theory (DFT) level using the program package TURBOMOLE 7.0.[46] The BH LYP functional was chosen for its better convergence compared to other hybrid functionals. All C, O, and H atoms were represented by the basis sets of triple zeta basis quality (def TZVP) and were treated at the all electron level.[46,47] The metal ion was represented by a 60 electron core pseudo potential (Np, ECP60MWB) with the corresponding basis sets of the triple zeta quality.[48] The complexes with different coordination modes (end on vs side on) of the ligand molecules were optimized. The gas phase energies E_g of the triplet ground states were computed on the MP2 level. For a theoretical approximation of the Gibbs free energies G, calculations of thermodynamic corrections ($E_{vib} = E_{zp} + H_0 - TS$, E_{zp} being the zero point energy, H_0 and S are the enthalpy and entropy obtained from calculations of the vibrational modes) and solvation energies E_{solv} (obtained using COSMO, r_{Np} = 1.72 Å) were performed. The Gibbs free energies were calculated as follows: $G = E_g + E_{vib} + E_{solv}$.[49−51] Due to the ionic form of the Np(V) complexes, a full second hydration shell was added and optimized to avoid the charge of the complexes to contact the COSMO cavity.

3. RESULTS AND DISCUSSION

3.1. Vis/NIR Absorption Spectroscopy. *3.1.1. Absorption Spectra.* The absorption spectra of Np(V) are displayed in Figure 1 as a function of the total ligand concentration ($[Mal^{2-}]_{total}$ and $[Succ^{2-}]_{total}$) at temperatures of 20 and 85 °C. At 20 °C and $I_m(NaClO_4)$ = 1.0 mol kg^{-1}, the absorption band of the NpO_2^+ aquo ion is located at 980.1 ± 0.1 nm with a molar attenuation coefficient of $\varepsilon_{20°C}$ = 396 ± 4 L mol^{-1} cm^{-1} and a full width at half maximum (fwhm) of 7.4 nm. This is in excellent agreement with literature data and corresponds to the E_{4g} to E_{2g} transition.[52−55] With increasing ligand concen

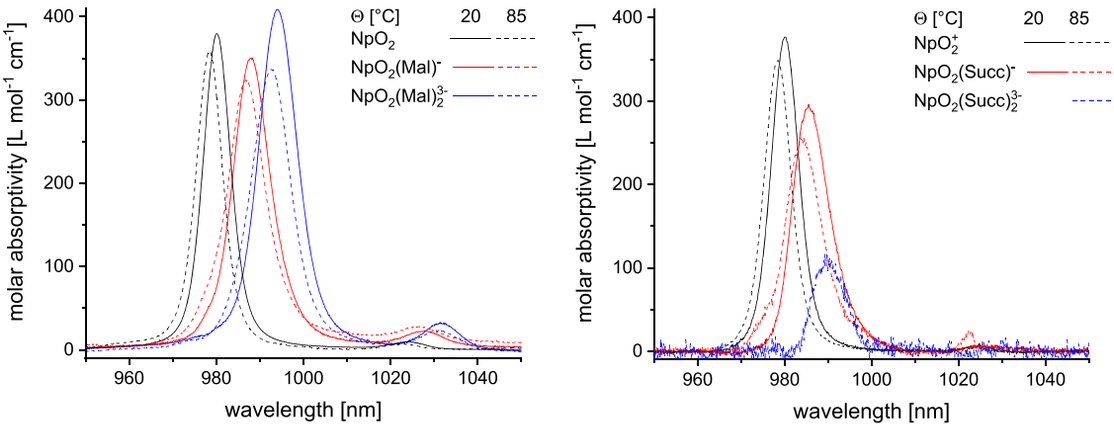

Figure 2. Absorption spectra of the solvated NpO_2^+ ion and the $NpO_2(L)_n^{1-2n}$ (n = 1, 2) [L^{2-} = Mal^{2-} (left), $Succ^{2-}$ (right)] complexes at Θ = 20 °C (solid lines) and 80° (dashed lines), $I_m(NaClO_4)$ = 1.0 mol kg^{-1}.

tration, a bathochromic shift of the absorption band is observed for both ligand systems. In the case of malonate, the bathochromic shift accompanies the formation of two additional absorption bands at 988.0 ± 0.1 and 994.1 ± 0.2 nm. This indicates that two NpO_2^+ malonate complexes are formed. With increasing succinate concentration, the bath ochromic shift is less pronounced and only a broadening of the absorption spectrum is observed. The fwhm increases from 7.4 to 12.4 nm. In addition, one isosbestic point at 983.1 ± 0.2 nm is observed. This indicates the formation of only one Np(V) succinate complex species. At 85 °C, the spectrum of the NpO_2^+ aquo ion shifts hypsochromically by 1.6 nm and the molar attenuation coefficient decreases $\varepsilon_{20°C}$ = from 396 ± 4 L mol^{-1} cm^{-1} to $\varepsilon_{85°C}$ = 374 ± 10 L mol^{-1} cm^{-1}. With increasing ligand concentration, a bathochromic shift is observed. This indicates the formation of NpO_2^+ complexes with malonate and succinate. In the case of malonate, the bathochromic shift at 85 °C is less pronounced compared to room temperature, and the two absorption bands of the complex species are also shifted by about 1.3 nm to longer wavelengths. The smaller bathochromic shift indicates a hindered complexation of Np(V) with malonate at elevated temperatures. In contrast, for the complexation of Np(V) with succinate, the fwhm at 85 °C increases from 7.4 to 13.2 nm with increasing $[Succ^2]_{total}$, indicating a favored complexation.

The temperature induced shift of the Np(V) absorption to shorter wavelengths was already observed in previous studies.[54,56−58] In the literature, this effect was explained by changes of the physical properties (e.g., dielectric constant, refractive index, polarity) of water with increasing temperature affecting the electronic absorption of the NpO_2^+ ions.[54,56] Also changes of the hydration in the first and second solvation sphere or changes of the complex geometries due to increasing temperatures might contribute to this shift.[57,58]

The temperature induced shift of the absorption band of the Np(V) ion to shorter wavelengths is contrary to the bathochromic shift of the spectra, which results from the complexation of Np(V) with malonate and succinate. Due to this temperature dependency of the absorption bands, each series of spectra must be treated separately, and single component spectra must be determined for all the studied experimental conditions.

3.1.2. Peak Deconvolution. The single component spectra of the Np(V) complexes with malonate and succinate are derived via subtractive peak deconvolution. Details on this procedure are given elsewhere.[59] Identical spectra are determined in NaCl and $NaClO_4$ media for the respective complex species at equal ionic strength. The single component spectra at 20 and 85 °C and $I_m(NaClO_4)$ = 1.0 mol kg^{-1} are displayed in Figure 2.

At 20 °C, the single component spectra of two different NpO_2^+ malonate complex species display absorption bands at 988.0 ± 0.1 and 994.1 ± 0.2 nm, which are hypsochromically shifted by 1.3 nm at 85 °C. In the case of succinate, only one absorption spectrum of a single NpO_2^+ succinate complex with an absorption maximum at 985.4 ± 0.1 nm is obtained at 20 °C. At 85 °C, the absorption band of this species is hypsochromically shifted by 1.7 nm and the absorption band of a second succinate complex with an absorption maximum at 989.7 ± 0.2 nm is observed. In Table 1, the spectroscopic parameters of the NpO_2^+ complexes with malonate and succinate are summarized for 20 and 85 °C.

Table 1. Spectroscopic Properties of the Species NpO_2^+, $NpO_2(Mal)^-$, $NpO_2(Mal)_2^{3-}$, $NpO_2(Succ)^-$, and $NpO_2(Succ)_2^{3-}$ at Θ = 20 and 85 °C

Θ [°C]	complex	λ_{max} [nm]	ε_{max} [L mol^{-1} cm^{-1}]	λ_{fwhm} [nm]
20	NpO_2^+	980.1 ± 0.1	396 ± 4	7.4 ± 0.4
	$NpO_2(Mal)^-$	988.0 ± 0.1	365 ± 14	10.1 ± 0.5
	$NpO_2(Mal)_2^{3-}$	994.1 ± 0.2	425 ± 16	10.5 ± 0.6
	$NpO_2(Succ)^-$	985.4 ± 0.1	311 ± 5	9.9 ± 0.5
85	NpO_2^+	978.4 ± 0.1	374 ± 10	7.3 ± 0.4
	$NpO_2(Mal)^-$	986.7 ± 0.2	337 ± 13	10.4 ± 0.6
	$NpO_2(Mal)_2^{3-}$	992.6 ± 0.2	348 ± 14	10.8 ± 0.6
	$NpO_2(Succ)^-$	983.7 ± 0.2	269 ± 13	9.7 ± 0.5
	$NpO_2(Succ)_2^{3-}$	989.7 ± 0.2	117 ± 6	8.6 ± 0.4

Comparing the positions of the absorption bands of the malonate and succinate complexes shows that the complex ation of NpO_2^+ with malonate results in a more pronounced bathochromic shift of approximately 7.3 nm for each coordinating ligand molecule compared to the complexation with succinate causing a bathochromic shift of only 5.6 nm per molecule. Furthermore, the effect of increasing temperature on the absorption bands of the malonate complexes is weaker compared to that of the NpO_2^+ succinate species.

3.1.3. Speciation and Complex Stoichiometry. The evolution of the different Np(V) malonate and succinate

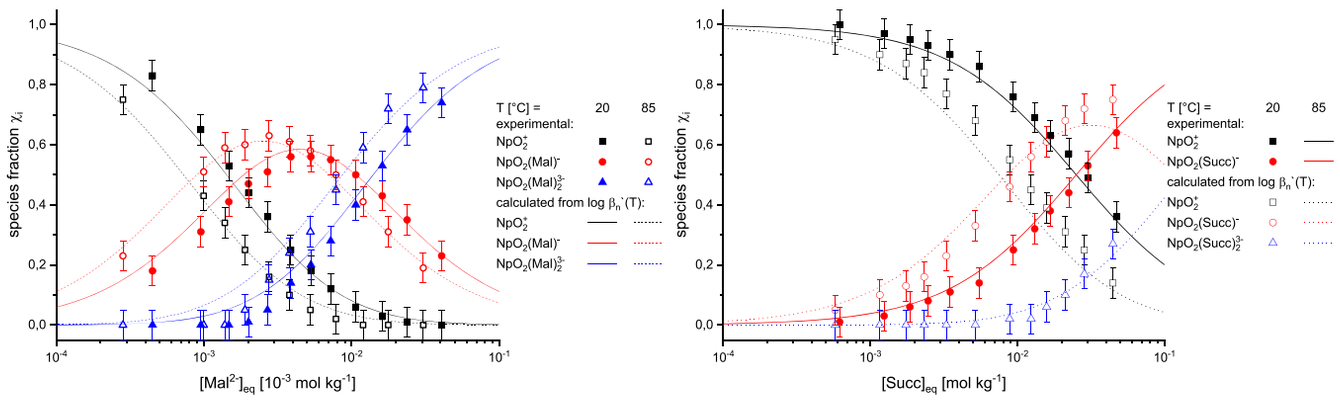

Figure 3. Experimentally determined (symbols) and calculated species distribution of the $NpO_2(L)_n^{1-2n}$ (n = 0, 1, 2; L^{2-} = Mal^{2-}, $Succ^{2-}$) complexes as a function of the equilibrium ligand concentration in aqueous solution. I_m = 1.0 $NaClO_4$; Θ = 20 °C (solid lines) and 85 °C (dashed lines).

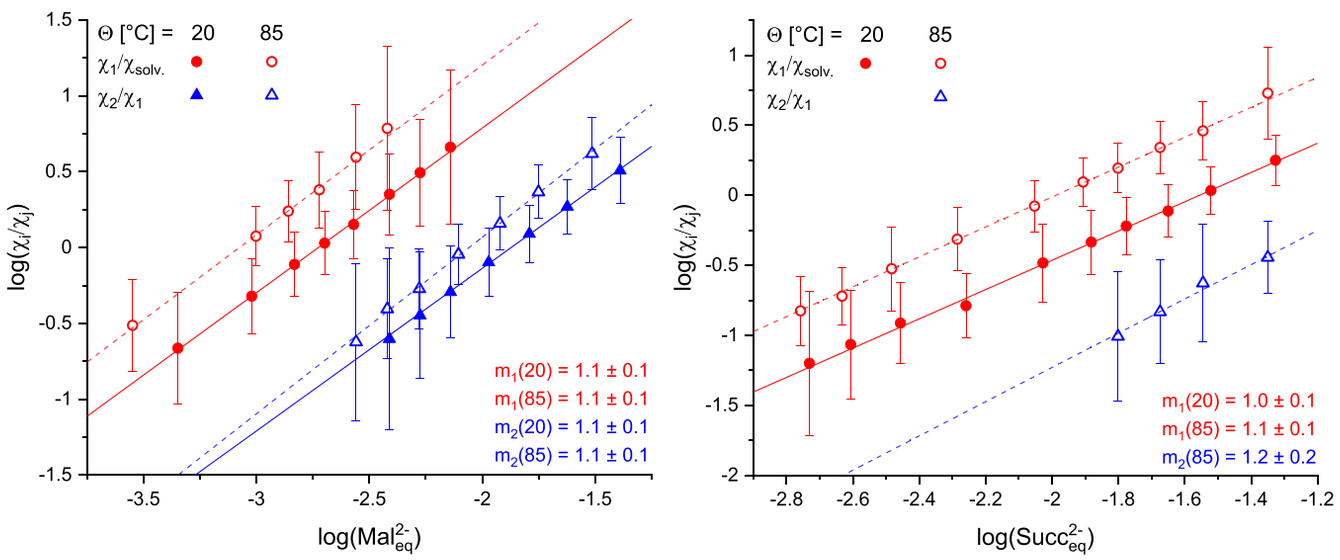

Figure 4. Plots of log ($[NpO_2(L)_n]^{1-2n}/[NpO_2(L)_{n-1}]^{3-2n}$) vs log ($[L^{2-}]_{eq}$) and linear regression analyses at Θ = 20, 85 °C and I_m = 1.0 mol kg^{-1} H_2O. (left): L^{2-} = Mal^{2-}, (right) L^{2-} = $Succ^{2-}$.

complexes as a function of the ligand concentration is derived by the iterative deconvolution of the measured absorption spectra. Principal component analysis is applied using the single component spectra derived at each experimental condition (Θ, I_m). Details on this procedure are given in the literature.[59,60] In Figure 3, the experimental (symbols) and calculated (lines) species distributions are displayed as a function of the equilibrium malonate and succinate concen trations $[L^{2-}]_{eq}$ for Θ = 20 and 85 °C at $I_m(NaClO_4)$ = 1.0 mol kg^{-1}. At 20 °C, the chemical equilibrium shifts toward the complexed Np(V) species with increasing ligand concentration and the formation of two malonate complexes and one succinate complex is observed. Furthermore, higher ligand concentrations and/or higher temperatures are required for succinate to form the two different complex species. This indicates a weaker complexation of Np(V) with succinate then with malonate. At 85 °C, the speciation shifts to lower ligand concentrations for both ligand systems. This indicates an endothermic complexation behavior.

The stoichiometry of the formed Np(V) malonate and succinate complexes is determined by slope analyses. The following complexation model (eq 1) is used

$$NpO_2^+ + L^{2-} \rightleftharpoons NpO_2(L)^-$$
$$NpO_2(L)^- + L^{2-} \rightleftharpoons NpO_2(L)_2^{3-}$$
$$\vdots$$
$$NpO_2(L)_{n-1}^{1-(2(n-1))} + L^{2-} \rightleftharpoons NpO_2(L)_n^{1-2n} \quad (1)$$

The logarithmic form of the law of mass action for the stepwise complex formation according to eq 1 is given in eq 2

$$\log K_n' = \log \frac{[NpO_2(L)_n]^{1-2n}}{[NpO_2(L)_{n-1}]^{1-(2(n-1))}} - 1 \cdot \log[L^{2-}]_{eq};$$
$$\beta_n' = \prod K_n' \quad (2)$$

with $[L^{2-}]_{eq}$ being the free, deprotonated malonate, or succinate concentration in solution at a given temperature and ionic strength. Plots of $\log \frac{[NpO_2(L)_n]^{1-2n}}{[NpO_2(L)_{n-1}]^{1-(2(n-1))}}$ versus $\log[L^{2-}]_{eq}$ are expected to yield a slope of one for each complexation step. For calculation of the equilibrium ligand concentration, the protonation reactions of malonate and

succinate and the formation of Na^+ complexes have to be considered

$$\log \beta_{A1}: L^{2-} + H^+ \rightleftharpoons HL^-$$
$$\log \beta_{A2}: HL^- + H^+ \rightleftharpoons H_2L$$
$$\log \beta_{Na}: L^{2-} + Na^+ \rightleftharpoons NaL^- \quad (3)$$

The equilibrium concentrations of L^{2-}, HL^-, H_2L, NaL^-, and H^+ are calculated with the software package Hyperquad Hyss2008, Version 4.0.31, as a function of $[L^{2-}]_{total} = [L^{2-}]_{eq} + [HL^-]_{eq} + [H_2L]_{eq} + [NaL^-]_{eq}$, $[H^+]_{total} = [H^+]_{eq} + [HL^-]_{eq} + 2 \times [H_2L]_{eq}$, I_m and Θ.[61] Hereby, the amount of the ligand complexed to the Np(V) is neglected, as the concentration on Np(V) is at least 1 order of magnitude lower than the ligand concentration. The temperature dependent thermodynamic stability constants $\log \beta_x(\Theta)$ of the reactions given in eq 3 are calculated using the integrated Van't Hoff equation with data reported in the literature.[62−67] The ionic strength dependence is taken into account by the specific ion interaction theory (SIT) as recommended by the Nuclear Energy Agency−Thermodynamic Database (NEA TDB).[68] The binary ion−ion interaction coefficients $\varepsilon_{j,k}$ are taken from the NEA TDB.[68]

The slope analyses for 20 and 85 °C (I_m = 1.0 mol kg^{-1}) are given in Figure 4. A linear correlation of $\log \frac{[NpO_2(L)_n]^{1-2n}}{[NpO_2(L)_{n-1}]^{1-(2(n-1))}}$ versus $\log[L^{2-}]_{eq}$ is observed, revealing slopes between 0.9 ± 0.1 and 1.2 ± 0.2 at all experimental conditions for both ligand systems. Thus, the formation of two different NpO_2^+ complexes with malonate and succinate with stoichiometries of $NpO_2(L)_n^{1-2n}$ and n = 1, 2 is confirmed. In the case of succinate, the formation of $NpO_2(Succ)_2^{3-}$ can only be observed for Θ > 50 °C.

3.1.4. Thermodynamic Data. To determine thermodynamic functions ($\log \beta_n^\circ(\Theta)$, $\Delta_R H_{m,n}^\circ$, and $\Delta_R S_{m,n}^\circ$) at IUPAC reference state conditions (I_m = 0, T = 298 K), a consistent set of conditional stability constants $\log \beta_n'(\Theta)$ at various I_m and Θ is required. Therefore, $\log \beta_n'(\Theta)$ values for the formation of $NpO_2(L)^-$ and $NpO_2(L)_2^{3-}$ are calculated according to the law of mass action (eq 2) at various temperatures and NaCl or $NaClO_4$ concentrations. These data are extrapolated to zero ionic strength (I_m = 0) according to eq 4, which gives the thermodynamic stability constants $\log \beta_n^\circ(\Theta)$.[68]

$$\log K'(\Theta) - \Delta z^2 D = \log K^\circ(\Theta) - \Delta\varepsilon I_m \quad (4)$$

D is the Debye−Hückel term, $\Delta z^2 = \sum z_{end}^2 - \sum z_{start}^2$ is the sum of the charges z, and $\Delta\varepsilon = \sum \varepsilon_{end} - \sum \varepsilon_{start}$ is the sum of the binary ion−ion interaction coefficients $\varepsilon_{j,k}$ of the reactants. For both ligand systems, a linear correlation of $\log \beta_n'(\Theta) - \Delta z^2 D$ versus I_m is observed for all studied temperatures. Equal $\log \beta_n^\circ(\Theta)$ values are obtained for both electrolytes (NaCl, $NaClO_4$) as expected due to the application of the SIT (see Supporting Information, Tables S1 and S2). Thus, averaged $\log \beta_n^\circ(\Theta)$ values are calculated for the respective malonate and succinate complexes. The averaged $\log \beta_n^\circ(\Theta)$ values are listed in Table 2.

In the case of malonate, an increase of $\log \beta_1^\circ$(20 °C) = 3.31 ± 0.07 to $\log \beta_1^\circ$(85 °C) = 3.61 ± 0.08 and of $\log \beta_2^\circ$(20 °C) = 3.90 ± 0.11 to $\log \beta_2^\circ$(85 °C) = 4.35 ± 0.12 is observed. For the complexation of Np(V) with succinate an increase of $\log \beta_1^\circ$(20 °C) = 2.13 ± 0.15 to $\log \beta_1^\circ$(85 °C) = 2.56 ± 0.22 and $\log \beta_2^\circ$(50 °C) = 1.14 ± 0.21 to $\log \beta_2^\circ$(85 °C) = 2.26 ± 0.24 is observed. A comparison of the results shows that the stability constants of $NpO_2(Succ)^-$ are by 1.1−1.2 orders of magnitude lower compared to $NpO_2(Mal)^-$, whereas the stability constants of $NpO_2(Succ)_2^{3-}$ are by 2.1−2.8 lower compared to those of the respective $NpO_2(Mal)_2^{3-}$ complex. These results confirm the observations that Np(V) forms weaker complexes with succinate than with malonate.

Table 2. Thermodynamic Stability Constants Log $\beta_n^\circ(T)$ for $NpO_2(L)_n^{1-2n}$ (n = 1, 2) with L^{2-} = Mal^{2-} and $Succ^{2-}$ as a Function of the Temperature

	Θ [°C]	Mal^{2-}	$Succ^{2-}$
$NpO_2^+ + L^2 \rightleftharpoons NpO_2(L)^-$	20	3.31 ± 0.07	2.13 ± 0.15
	30	3.41 ± 0.08	2.11 ± 0.14
	40	3.42 ± 0.09	2.12 ± 0.10
	50	3.51 ± 0.08	2.19 ± 0.10
	60	3.50 ± 0.09	2.26 ± 0.12
	70	3.54 ± 0.08	2.36 ± 0.11
	80	3.56 ± 0.09	2.53 ± 0.20
	85	3.61 ± 0.08	2.56 ± 0.22
$NpO_2^+ + 2L^2 \rightleftharpoons NpO_2(L)_2^{3-}$	20	3.90 ± 0.11	
	30	3.99 ± 0.08	
	40	4.04 ± 0.10	
	50	4.20 ± 0.09	1.41 ± 0.21
	60	4.20 ± 0.14	1.67 ± 0.15
	70	4.25 ± 0.11	1.77 ± 0.16
	80	4.30 ± 0.11	2.00 ± 0.22
	85	4.35 ± 0.12	2.26 ± 0.24

The determination of the standard reaction enthalpies $\Delta_r H_{n,m}^\circ$ and entropies $\Delta_r S_{n,m}^\circ$ of the respective complexation reactions is performed according to the integrated Van't Hoff equation given in eq 5.[62]

$$\log \beta_n^\circ(\Theta) = \log \beta_n^\circ(\Theta_0) + \frac{\Delta_r H_{n,m}^\circ(\Theta_0)}{R \ln(10)}\left(\frac{1}{\Theta_0} - \frac{1}{\Theta}\right) \quad (5)$$

R is the universal gas constant. In Figure 5, the standard stability constants $\log \beta_n^\circ(\Theta)$ are plotted versus the reciprocal temperature T^{-1}. The data show a linear correlation. The standard reaction enthalpies are obtained from the slopes of the linear regression analyses ($\log \beta_n^\circ(\Theta) = m \times T^{-1} + C$): $\Delta_r H_{n,m}^\circ = -m_n \times R \times \ln(10)$. The standard reaction entropies are calculated from the intercepts of the y axis: $\Delta_r S_{n,m}^\circ = C \times R \times \ln(10)$.

All complexation reactions have positive $\Delta_r H_{n,m}^\circ$ values indicating an endothermic complexation driven by the gain of entropy. In Table 3, the determined thermodynamic functions ($\Delta_r H_{n,m}^\circ$ and $\Delta_r S_{n,m}^\circ$) and thermodynamic stability constants at 25 °C are summarized and compared to literature data given by the NIST standard reference database.[69] The given thermodynamic stability constants for $NpO_2(Mal)^-$ ($\log \beta_1^\circ$ = 3.16) and $NpO_2(Succ)^-$ ($\log \beta_1^\circ$ = 2.13) are in an excellent agreement with the results of the present work. Unfortunately, no $\Delta_r H_{m,1}^\circ$ and $\Delta_r S_{m,1}^\circ$ values are given for these complexes.

To investigate steric effects, the results for the Np(V) complexes of the present work are compared to recently published data for the complexation of Np(V) with oxalate (Ox^{2-}).[70] A comparison of $\log \beta_n^\circ(\Theta)$ of oxalate, malonate, and succinate reveals a successive decrease of the complex stability with increasing C backbone of the dicarboxylates. For $NpO_2(L)^-$, $\log \beta_1^\circ$(25 °C) decreases by approximately 1.2

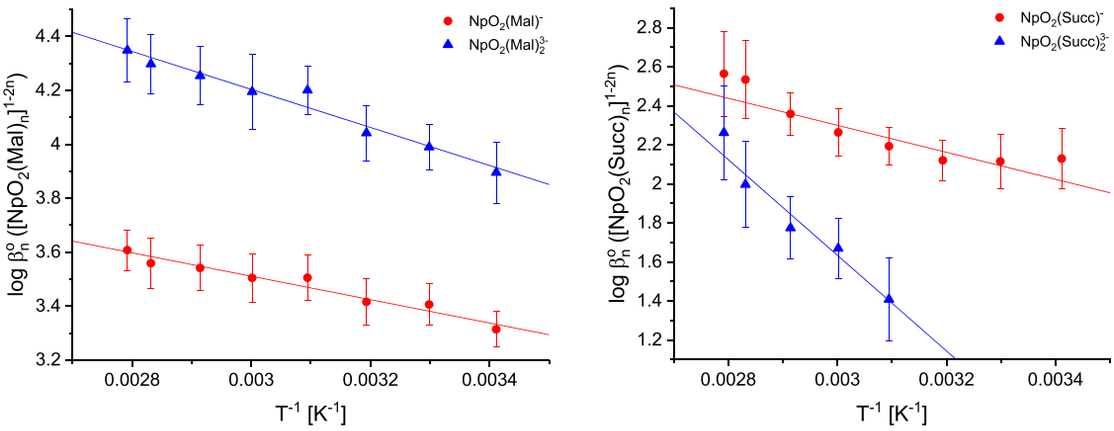

Figure 5. Plots of log $\beta_n^\circ(T)$ (n = 1, 2) as a function of the reciprocal temperature and fittings according to the integrated Van't Hoff equation.

Table 3. Thermodynamic Stability Constants, Enthalpies, and Entropies of Reaction for the Complexation of Np(V) with Oxalate, Malonate, and Succinate at Ionic Strength I = 0 and Θ = 25 °C[a]

complex	log β_i° (25 °C)	$\Delta_r H_{n,m}^\circ$ [kJ mol^{-1}]	$\Delta_r S_{n,m}^\circ$ [J mol^{-1} K^{-1}]	refs
$NpO_2(Ox)^-$	4.53 ± 0.12	1.3 ± 0.7	83 ± 2	70
$NpO_2(Ox)_2^{3-}$	6.22 ± 0.24	8.7 ± 1.4	90 ± 5	70
$NpO_2(Mal)^-$	3.36 ± 0.11	8.3 ± 0.7	92 ± 2	p.w.
	3.16			69
$NpO_2(Mal)_2^{3-}$	3.95 ± 0.19	13.5 ± 1.1	121 ± 3	p.w.
$NpO_2(Succ)^-$	2.05 ± 0.45	13.2 ± 2.7	83 ± 8	p.w.
	2.13			69
$NpO_2(Succ)_2^{3-}$	0.75 ± 1.22	47.0 ± 7.4	172 ± 22	p.w.

[a]p.w.: present work.

from oxalate to malonate and by 1.3 from malonate to succinate. In the case of $NpO_2(L)_2^{3-}$, the decrease is even stronger. From oxalate to malonate, log β_2°(25 °C) decreases by 2.3 and from malonate to succinate by 3.2. A similar trend is observed for the standard reaction enthalpies. The formation of $NpO_2(Ox)_n^{1-2n}$ is exothermic, whereas the formation of $NpO_2(Mal)_n^{1-2n}$ is weakly endothermic and an additional increase of $\Delta_r H_{n,m}^\circ$ is observed for $NpO_2(Succ)_n^{1-2n}$ (see Table 3). Our structural investigations (see section below) show that these trends originate from changes in the coordination mode in the series oxalate, malonate, and succinate with the NpO_2^+ ion.

Additionally, the SIT modeling of the ionic strength dependence of log $\beta_n'(\Theta)$ reveals the sum of the binary ion–ion interaction coefficients $\Delta\varepsilon_n^\circ(\Theta)$ as a function of the temperature for the background electrolytes, NaCl and $NaClO_4$. In Figure 6, the $\Delta\varepsilon_n^\circ(\Theta)$ values are displayed as a function of the temperature for $NpO_2(Mal)_n^{1-2n}$ and $NpO_2(Succ)_n^{1-2n}$. In all systems, no significant temperature dependence of $\Delta\varepsilon_n^\circ(\Theta)$ is observed and averaged, temperature independent $\Delta\varepsilon_n^\circ$ values are calculated (given as solid lines). This is in good agreement with the negligible temperature dependence of $\Delta\varepsilon_n^\circ(\Theta)$ values for Np(V) and An(III) complexes with various organic and inorganic ligands described in the literature .[23,32,53,54,56,71,72] The binary ion–ion interaction coefficients $\varepsilon_{j,k}$ of the $NpO_2(L)_n^{1-2n}$ complexes (L^{2-} = Mal^{2-}, $Succ^{2-}$) with Na^+ are calculated according to the SIT using eq 6 and the interaction coefficients $\varepsilon(NpO_2^+, ClO_4^-)$ = 0.25 ± 0.05 and $\varepsilon(NpO_2^+, Cl^-)$ = 0.09 ± 0.05 given in the NEA TDB. The values of $\varepsilon(Na^+, Mal^{2-})$ = −0.05 ± 0.03 and $\varepsilon(Na^+, Succ^{2-})$ = 0.09 ± 0.02 are calculated from literature data using the SIT procedure.[63,64,73]

$$\Delta\varepsilon = \sum \varepsilon_{\text{products}} - \sum \varepsilon_{\text{educts}} \qquad (6)$$

The $\varepsilon_{j,k}$ values are given in Table 4. According to the SIT, identic $\varepsilon_{j,k}$ values should be obtained for the respective complexes regardless of the used background electrolyte. This is not the case for $NpO_2(Mal)_n^{1-2n}$ and $NpO_2(Succ)_n^{1-2n}$ (n = 1, 2) as slight deviations are observed for the values determined in NaCl or $NaClO_4$ media. In previous studies, it was shown that these discrepancies originate from a defective $\varepsilon(NpO_2^+, ClO_4^-)$ = 0.25 ± 0.05 reported in the NEA TDB.[53,56,72,73] Nevertheless, the log $\beta_n^\circ(\Theta)$ of the respective complex species obtained in NaCl or $NaClO_4$ are in excellent agreement. Thus, the ionic strength dependence of log $\beta_n^\circ(\Theta)$ is accurately described with the $\Delta\varepsilon_n^\circ$ determined in this work.

3.2. Structure and Coordination Modes. The observed trends within spectroscopic properties and the thermodynamic data in the series Np(V) oxalate, malonate, and succinate are expected to originate from different coordination modes of the ligands toward the metal center (see Scheme 1). Malonate and succinate can either coordinate with only one COO^- group toward the Np(V) ion (end on; bidentate coordination with both O atoms of one COO^- group) or they form chelate rings with both COO^- groups coordinating to the metal center (side on; monodentate coordination with one O atom of each COO^- group).

3.2.1. ATR-FT-IR Spectroscopy. Information on the coordination mode of Np(V) with dicarboxylic acids can be derived from the vibrational modes of the ligands and the NpO_2^+ ion. Prior to the analysis of the NpO_2^+ complexes, the vibrational absorption spectra of the dissolved ligands at the selected pD values are recorded (Figure 7 top). At low pD values, the spectra of the free ligands show strong absorption bands at ~1700 cm^{-1}, which decrease with increasing pD and are not observed at neutral pD values. These bands are assigned to the stretching vibrational mode of the COOD groups of the dicarboxylic acids. Furthermore, bands between 1565 and 1580 cm^{-1} and between 1350 and 1410 cm^{-1} are observed. These bands represent the antisymmetric [$\nu_{as}(COO^-)$] and symmetric [$\nu_s(COO^-)$] stretching modes of the COO^- group, respectively.[74]

The infrared spectra of the Np(V) complex species at pD values between 4.0 and 7.4 are shown in Figure 7 (bottom).

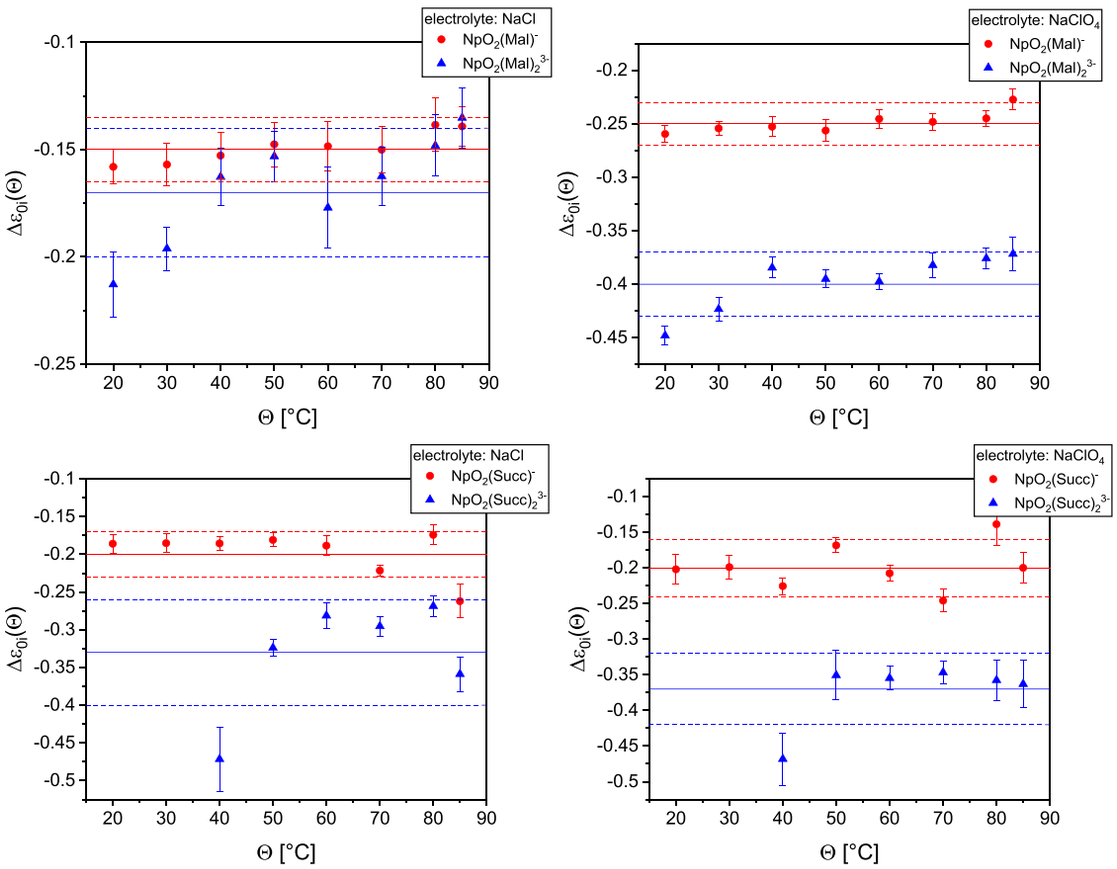

Figure 6. $\Delta\varepsilon_{j,k}(\Theta)$ values for the formation of $[NpO_2(L)_n]^{1-2n}$ (n = 1, 2; L^{2-} = Mal^{2-}, $Succ^{2-}$) in NaCl (left) and $NaClO_4$ (right) as a function of the temperature. The error bars (dashed lines) equal the 1σ error of the mean value (dashed lines).

Table 4. Temperature Independent Binary Ion−Ion Interaction Coefficients $\varepsilon_{j,k}$ for the Formation of $NpO_2(L)_n^{1-2n}$ (n = 1, 2; L^{2-} = Mal^{2-}, $Succ^{2-}$) in NaCl and $NaClO_4$ Media

electrolyte	$NpO_2(Mal)^-$	$NpO_2(Succ)^-$	$NpO_2(Mal)_2^{3-}$	$NpO_2(Succ)_2^{3-}$
NaCl	0.12 ± 0.06	0.02 ± 0.04	0.20 ± 0.06	0.06 ± 0.08
$NaClO_4$	0.06 ± 0.04	0.14 ± 0.04	0.27 ± 0.05	0.06 ± 0.06

Scheme 1. Structures of the 1:1 Np(V) Complexes with Malonate (n = 1) and Succinate (n = 2) with Different Coordination Modes[a]

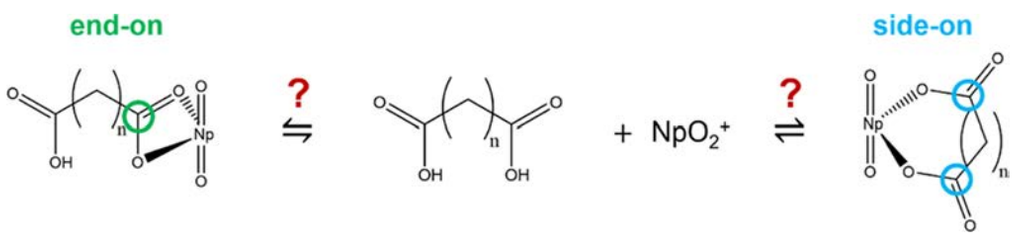

[a]Left: end on coordination with a bidentate coordinating COO^- group; right: side on coordination with monodentate coordination of both COO^- groups.

These difference spectra were calculated from single beam spectra of the Np(V) complex solution and the free ligand solution at identical experimental conditions. This results in a minimization of the constant parts of the spectra, which involves, in particular, the strong absorbing background from the bulk water and contributions from the experimental setup. The complexation of Np(V) with malonate and succinate results in changes in the electron density distribution within the COO^- groups and the Np═O bonds leading to characteristic changes in the respective vibrational modes. These changes are observed as negative and positive bands in the difference spectra.

The negative absorption bands at ~1700 cm^{-1} in the spectra at low pD_c conditions are attributed to carboxyl groups of the uncomplexed malonic and succinic acids. Due to the complexation of the Np(V) ion with Mal^{2-}, the protonation equilibrium of the ligand is shifted toward the deprotonated ligand species Mal^{2-}, which is reflected by the negative

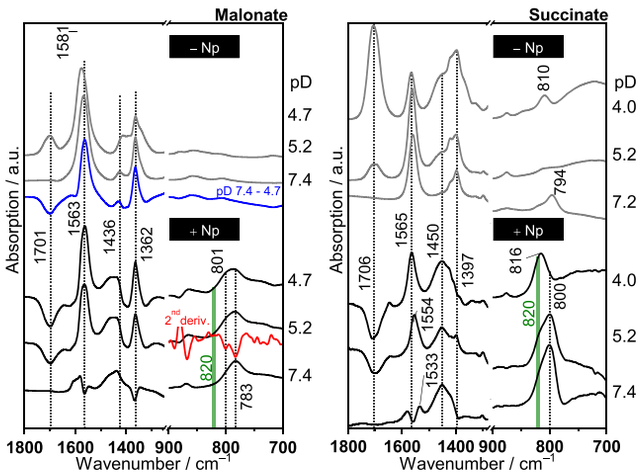

Figure 7. Mid IR spectra of the aqueous deuterated solutions of malonate (left) and succinate (right) in the absence (−Np) and presence (+Np) of Np(V) at different pD values {[Np] = 2 mmol kg^{-1} (Mal^{2-}) and 1 mmol kg^{-1} for ($Succ^{2-}$) and $[Mal^{2-}/Succ^{2-}]_{tot}$ = 0.1 mol kg^{-1}, I_m = 1.0 mol kg^{-1} (Na^+, $Mal^{2-}/Succ^{2-}/Cl^-$)}.

absorption band of the C═O stretching vibration at ~1700 cm^{-1}. This is verified by the difference spectrum calculated from the spectra of the malonate ligand recorded at pD 7.4 and 4.7 (blue trace in Figure 7) also showing a negative band in the frequency range >1350 cm^{-1}. Comparable results are obtained for succinate.

The positive bands at 1563 and 1362 cm^{-1} in the malonate spectra (Figure 7 bottom, left) and 1565 and 1397 cm^{-1} in the succinate spectra (Figure 7 bottom, right) represent modes of the carboxylate groups in the Np(V) complexes. For both ligands, a shift of the antisymmetric stretching mode $\nu_{as}(COO^-)$ to lower wavenumbers is observed. For malonate, the shift is 18 cm^{-1} from 1581 to 1563 cm^{-1}. For succinate, $\nu_{as}(COO^-)$ shifts about 11 cm^{-1} from 1565 to 1554 cm^{-1}. These spectral shifts indicate a change in the electron density within the COO^- group caused by the strong ionic character of the NpO_2^+—ligand bond. In contrast, the frequency of the symmetrical stretching vibrational mode $\nu_{as}(COO^-)$ appears less sensitive with respect to the ionic interactions with Np(V), as the frequencies of these modes are observed in all spectra at 1362 and 1397 cm^{-1}.

An assignment of the coordination mode of the ligand to a complexing metal ion can be potentially derived from the spectral splitting of the $\nu_{as}(COO^-)$ and $\nu_s(COO^-)$ stretching modes.[75] The splitting of ~200 cm^{-1} in the case of Np(V) malonate suggests a monodentate coordination of the COO^- group to the Np(V) ion excluding an end on coordination mode (see Scheme 1). Consequently, the considerably lower splitting in the series of the Np(V) succinate spectra indicates a different kind of coordination, namely, an end on coordination.

In addition to the vibrational modes of the ligands, the antisymmetric stretching vibrational mode $\nu3$(Np═O) gives valuable hints on the complex stoichiometry. For the free Np(V) ion, it occurs at 820 cm^{-1}.[30,76] Upon complex formation, the band is considerably shifted to a lower wavenumber, which is explained by the ionic character of the Np(V) carboxylate bond resulting in a change of the charge density between Np and the axial O atoms.

Upon complexation with malonate, at pD 4.7 and 5.2, a broad band is observed at around 790 cm^{-1}. The second derivative reveals two peaks at 801 and 783 cm^{-1} corresponding to the $NpO_2(Mal)_n^{1-2n}$ (n = 1, 2) complexes for this band. Upon increasing the pD up to 7.4, the band shows a symmetric shape centering at 783 cm^{-1} showing the predominance of $NpO_2(Mal)_2^{3-}$.

Upon complexation with succinate, $\nu3$(Np═O) is only slightly shifted by 4 cm^{-1} at pD 4.0. With increasing pD from 4.0 to 5.2 and finally 7.4, the band shows a bathochromic shift to 800 cm^{-1}. At pD 7.4, the symmetric shape of the $\nu3$(Np═O) bands suggest the predominance of one species which is assigned to $NpO_2(Succ)^-$.

3.2.2. EXAFS Spectroscopy. Information on the bond distances and the coordination mode of the ligands in the respective $NpO_2(L)_n^{1-2n}$ complexes are determined by EXAFS spectroscopy. Np L_3 EXAFS spectra of Np(V) in the presence of malonate or succinate are recorded as a function of the pH_c value. The k^2 weighted Np L_3 EXAFS spectra, the Fourier Transformations, and the fit curves are displayed in Figures S1 and S2 in the Supporting Information. Detailed results and the respective fitting parameters are given in the Supporting Information (Tables S3 and S4). In Table 5, the distances

Table 5. Distances (in Å) of the Coordinating Fist Shell O Atoms and of the C Atoms of Coordinating COO^- Groups in the $NpO_2(L)_n^{1-2n}$ (n = 1, 2, L^{2-} = Mal^{2-}, $Succ^{2-}$) Complexes Obtained by EXAFS Spectroscopy

	propionate[32]	oxalate[70]	malonate [p.w.]	succinate [p.w.]
O_{ax}	1.82(1)	1.83(1)	1.85(1)	1.83(1)
O_{eq}	2.47(1)	2.45(2)	2.48(2)	2.48(2)
C_c	2.87(3)	3.32(3)	3.41(4)	2.83(5)

between the ligand atoms and the Np(V) center are summarized. The results show that for the axial O atoms (O_{ax}) of the Np(V) complexes, an averaged distance of 1.84 ± 0.01 Å is obtained. For the equatorial O atoms (O_{eq}), the average distance is 2.47 ± 0.02 Å and the coordination number in the equatorial plane counts for 3.5−5.1 through the series of samples. These results are in excellent agreement with literature data.[37,77] The coordination mode of the dicarboxylates is determined using the distances of the C atoms of the coordinating carboxylic groups C_c. For the malonate complexes, the C_c distance is 3.41 ± 0.03 Å and for the succinate complexes, it is 2.83 ± 0.04 Å. Thus, distinctively longer C_c distances are obtained for the $NpO_2(Mal)_n^{1-2n}$ complexes compared with $NpO_2(Succ)_n^{1-2n}$. This difference indicates different coordination modes. In the literature, two C_c distances are reported for the Np(V) acetate and−propionate complexes, which are 2.91 ± 0.02 and 2.87 ± 0.03 Å.[32,78] These monocarboxylic ligands coordinate via one COO^- group toward the Np(V) ion and thus, these C_c distances serve as a reference for an end on binding mode. The present result for succinate is in excellent agreement with the data for the acetate and propionate complexes confirming an end on coordination of succinate. In contrast, the C_c distance in the malonate complexes are by 0.50−0.58 Å longer, indicating the formation of chelate rings involving one O atom of each COO^- group. Furthermore, the C_c distance in the $NpO_2(Mal)_n^{1-2n}$ complexes is in excellent agreement with the results for Np(V) oxalate complexes also displaying side on coordination (C_c: 3.32 ± 0.06 Å).[70]

Table 6. Distances of the Ligand Atoms toward the Np(V) Ion Obtained from Structure Optimizations on the DFT Level and Comparison with the EXAFS Results

method	complex	coord. mod.	O_{ax} [Å]	O_{eq} [Å]	C_c [Å]
DFT	$NpO_2(Mal)^-$	end-on	1.82	2.49	2.88
		side-on	1.82	2.46	3.44
	$NpO_2(Mal)_2^{3-}$	end-on	1.82	2.48	2.90
		side-on	1.83	2.44	3.47
EXAFS	$NpO_2(Mal)^-/NpO_2(Mal)_2^{3-}$		1.85 ± 0.01	2.48 ± 0.02	3.41 ± 0.04
DFT	$NpO_2(Succ)^-$	end-on	1.81	2.47	2.86
		side-on	1.82	2.46	3.49
	$NpO_2(Succ)_2^{3-}$	end-on	1.80	2.51	2.92
		side-on	1.82	2.50	3.53
EXAFS	$NpO_2(Succ)^-/NpO_2(Succ)_2^{3-}$		1.83 ± 0.01	2.48 ± 0.02	2.83 ± 0.05

Table 7. Gibbs Free Energies for the Rearrangement of an End On into a Side On Coordinated Ligand Molecule

complex	ΔE_g [kJ mol^{-1}]	ΔE_{vib} [kJ mol^{-1}]	ΔE_{solv} [kJ mol^{-1}]	ΔG [kJ mol^{-1}]
$NpO_2(Mal)^-$	11.14	8.70	4.35	1.91
$NpO_2(Mal)_2^{3-}$	44.02	25.00	37.31	31.70
$NpO_2(Succ)^-$	5.25	14.22	22.34	41.81
$NpO_2(Succ)_2^{3-}$	87.40	43.67	28.64	15.09

3.2.3. Quantum Chemical Calculations. The experimentally determined coordination modes and structural data are supported by quantum chemical calculations. The structures of the fivefold $NpO_2(Mal)_n^{1-2n}$ and $NpO_2(Succ)_n^{1-2n}$ complexes (compare Scheme 1) are optimized. In the equatorial plane of the complexes, 3 or 1 water molecules for $NpO_2(L)^-$ or $NpO_2(L)_2^{3-}$ are added to obtain the coordination number of 5 in the equatorial plane. In Table 6, the results are summarized and compared with the experimentally determined distances. For both systems, the O_{ax} and O_{eq} distances are in excellent agreement with the experimental results. Furthermore, the calculations reveal a C_c distance for $NpO_2(Mal)_n^{1-2n}$ of 3.44 Å (n = 1) and 3.47 Å (n = 2) for side on coordinating ligand molecules. This is in perfect accordance with the EXAFS results. In the case of $NpO_2(Succ)_n^{1-2n}$, C_c distances of 2.86 Å (n = 1) and 2.92 Å (n = 2) are obtained hinting to an end on coordination. Thus, the interpretation of the EXAFS results is confirmed by the obtained distances from structure optimizations.

Theoretical approximations of the Gibbs free energies ΔG for the rearrangement of an end on into a side on coordinating ligand molecule according to Scheme 1 support the side on coordination for malonate and end on coordination for succinate. The ΔG values are calculated according to eq 7.

$$\begin{aligned}\Delta G &= G_{\text{end-on}} - G_{\text{side-on}} = E_{g(\text{end-on})} - E_{g(\text{side-on})} \\ &+ E_{vib(\text{end-on})} - E_{vib(\text{side-on})} + E_{solv(\text{end-on})} - E_{solv(\text{side-on})} \\ &= \Delta E_g + \Delta E_{vib} + \Delta E_{solv} \end{aligned} \quad (7)$$

E_g are the ground state energies of the complexes calculated on the MP2 level, E_{vib} considers thermodynamic corrections obtained from the calculations of the vibrational modes and E_{solv} describes solvation effects which are calculated using COSMO. The results are listed in Table 7.

The calculated ΔG values show negative values for both $NpO_2(Mal)_n^{1-2n}$ complexes, indicating an energetically preferred side on coordination of malonate. In contrast, for both $NpO_2(Succ)_n^{1-n}$ complexes, positive ΔG values are obtained indicating the preferred end on coordination of succinate. Thus, the theoretical approximations of ΔG for an end on into a side on rearrangement of the ligand also confirm the results by EXAFS and ATR FT IR spectroscopy for both ligands.

4. SUMMARY AND CONCLUSIONS

The present work is a detailed spectroscopic and thermodynamic study on the formation of Np(V) malonate and succinate complexes, giving standard state stability constants [$\log \beta_n^\circ(\Theta)$] and thermodynamic functions ($\Delta_r H_{n,m}^\circ$, $\Delta_r S_{n,m}^\circ$) as well as structural information on bond lengths and coordination modes of the ligands. For the determination of thermodynamic data, the complexation is studied by a systematic variation of the ligand concentration {$[Mal^{2-}]_{total}$, $[Succ^{2-}]_{total}$}, the ionic strength I_m (NaCl and $NaClO_4$ media), and the temperature (20−85 °C), using absorption spectroscopy in the near infrared region. The formation of exclusively $NpO_2(Mal)_n^{1-2n}$ and $NpO_2(Succ)_n^{1-2n}$ (n = 1, 2) is observed at all studied conditions. The stoichiometry of the formed complexes is confirmed by slope analyses according to the law of mass action. Both complexation reactions are endothermic representing shifts of the chemical equilibrium toward the complexed Np(V) species with increasing temperature. This is also reflected by an increase of the stability constants. In the case of malonate, the $\log \beta_1^\circ(20\ ^\circ C) = 3.31 \pm 0.07$ increases by 0.30 and $\log \beta_2^\circ(20\ ^\circ C) = 3.90 \pm 0.11$ by 0.45. For $NpO_2(Succ)^-$, $\log \beta_1^\circ(20\ ^\circ C) = 2.13 \pm 0.15$ increases by 0.43. The formation of $NpO_2(Succ)_2^{3-}$ is only observed at temperatures higher than 50 °C. The integrated Van't Hoff equation is used for the calculation of the standard reaction enthalpies and standard reaction entropies as the stability constants correlate linearly with T^{-1}. The calculations reveal positive $\Delta_r H_{n,m}^\circ$ values for all reactions being driven by the gain of entropy.

Structural information about bond distances of the complexes and coordination modes of the ligands are obtained by EXAFS spectroscopy, ATR FT IR spectroscopy, and quantum chemical calculations. The results reveal different coordination modes for malonate and succinate toward the Np(V) ion. For malonate, a side on coordination and the formation of six membered chelate rings is observed whereas

succinate coordinates end on via only one COO^- group. Thus, the formation of seven membered chelate rings in the equatorial plane of the Np(V) ion is energetically unfavorable.

The present work gives detailed information on the thermodynamic functions for the complexation reactions of Np(V) with malonate and succinate, providing data at IUPAC reference state conditions. The results are a valuable contribution to the thermodynamic database of actinides and help to improve the scientific basis, which is required for a comprehensive description of the aquatic chemistry of actinide ions. Furthermore, extensive effort is made to clarify the structures of the formed complex species by the application of EXAFS, ATR FT IR spectroscopy, and quantum chemical calculations. The studied ligand systems serve as models to investigate the effect of steric hindrance in the coordination of Np(V) with macromolecular organic compounds. Thus, the derived data improve the knowledge of actinide organic matter interaction at a molecular level.

ASSOCIATED CONTENT

Supporting Information

The Supporting Information is available free of charge at https://pubs.acs.org/doi/10.1021/acs.inorgchem.1c01966.

Determined thermodynamic standard state stability constants [$\log \beta_n^\circ(T)$] of the complexes of NpO_2^+ with malonate and succinate as a function of the temperature (20−85 °C), determined in $NaClO_4$ and NaCl media, parameters used for the fitting of the EXAFS spectra of NpO_2^+ (raw Np L_3 edge, k^2 weighted) determined in the malonate containing solution at different pH, parameters for the axial and equatorial oxygen atoms, as well as the multiscattering path of the axial oxygen atoms and carbon atoms of the carboxylic group of the ligand, parameters used for the fitting of the EXAFS spectra of NpO_2^+ (raw Np L_3 edge, k^2 weighted) determined in the succinate containing solution at different pH, parameters for the axial and equatorial oxygen atoms, as well as the multiscattering path of the axial oxygen atoms and carbon atoms of the carboxylic group of the ligand, recorded EXAFS spectra of Np(V) (raw Np L_3 edge, k^2 weighted) in malonate containing solution at different pH values, as well as the related Fourier transforms, and best fit using software EXAFSPAK, recorded EXAFS spectra of Np(V) (raw Np L_3 edge, k^2 weighted) in the succinate containing solution at different pH values, as well as the related Fourier transforms, and best fit using software EXAFSPAK (PDF)

AUTHOR INFORMATION

Corresponding Author

Andrej Skerencak Frech − *Karlsruher Institut für Technologie (KIT), Institut für Nukleare Entsorgung (INE), 76344 Eggenstein Leopoldshafen, Germany;* orcid.org/0000 0003 2177 4462; Email: andrej.skerencak@kit.edu

Authors

Martin M. Maiwald − *Ruprecht Karls Universität Heidelberg, Physikalisch Chemisches Institut, 69120 Heidelberg, Germany; Karlsruher Institut für Technologie (KIT), Institut für Nukleare Entsorgung (INE), 76344 Eggenstein Leopoldshafen, Germany*

Katharina Müller − *Helmholtz Zentrum Dresden Rossendorf, Institut für Ressourcenökologie, 01328 Dresden, Germany;* orcid.org/0000 0002 0038 1638

Karsten Heim − *Helmholtz Zentrum Dresden Rossendorf, Institut für Ressourcenökologie, 01328 Dresden, Germany*

Jörg Rothe − *Karlsruher Institut für Technologie (KIT), Institut für Nukleare Entsorgung (INE), 76344 Eggenstein Leopoldshafen, Germany;* orcid.org/0000 0001 5366 2129

Kathy Dardenne − *Karlsruher Institut für Technologie (KIT), Institut für Nukleare Entsorgung (INE), 76344 Eggenstein Leopoldshafen, Germany*

André Rossberg − *Helmholtz Zentrum Dresden Rossendorf, Institut für Ressourcenökologie, 01328 Dresden, Germany*

Carsten Koke − *Ruprecht Karls Universität Heidelberg, Physikalisch Chemisches Institut, 69120 Heidelberg, Germany*

Michael Trumm − *Karlsruher Institut für Technologie (KIT), Institut für Nukleare Entsorgung (INE), 76344 Eggenstein Leopoldshafen, Germany*

Petra J. Panak − *Ruprecht Karls Universität Heidelberg, Physikalisch Chemisches Institut, 69120 Heidelberg, Germany; Karlsruher Institut für Technologie (KIT), Institut für Nukleare Entsorgung (INE), 76344 Eggenstein Leopoldshafen, Germany*

Notes

The authors declare no competing financial interest.

ACKNOWLEDGMENTS

All IR spectroscopic measurements were carried out at the Institute of Resource Ecology at the Helmholtz Zentrum Dresden Rossendorf. Dr. H. Foerstendorf is acknowledged for the helpful discussion regarding the IR spectroscopic data. All absorption spectroscopic measurements were carried out at the Institute for Nuclear Waste Disposal (INE) at the Karlsruhe Institute of Technology (KIT). Dr. D. Fellhauer and Dr. M Altmaier are acknowledged for providing ^{237}Np and their experimental support. The KIT Institute for Beam Physics and Technology (IBPT) is acknowledged for the operation of the storage ring, the Karlsruhe Research Accelerator (KARA), and provision of the beamtime at the KIT light source. The European Synchrotron Radiation Facility (ESRF) is acknowl edged for the operation of the light source and provision of the beamtime at the ROBL beamline. This work is supported by the German Federal Ministry for Economic Affairs and Energy (BMWI) under contract 02E11415H and the German Federal Ministry of Education and Research (BMBF) under contract 02NUK039C.

REFERENCES

(1) Geckeis, H.; Röhlig, K. J.; Mengel, K. Endlagerung radioaktiver Abfälle. *Chem. Unserer Zeit* **2012**, *46*, 282−293.

(2) Runde, W. The chemical interactions of actinides in the environment. *Los Alamos Sci.* **2000**, *26*, 392−411.

(3) OECD. *Considering Timescales in the Post closure Safety of Geological Disposal of Radioactive Waste*; Agency, N. E., 2009.

(4) Gens, R.; Lalieux, P.; Preter, P. D.; Dierckx, A.; Bel, J.; Boyazis, J. P.; Cool, W. The Second Safety Assessment and Feasibility Interim Report (SAFIR 2 Report) on HLW Disposal in Boom Clay: Overview of the Belgian Programme. *MRS Proc.* **2011**, *807*, 917−924.

(5) Oecd, N. E. A. *Safety of Geological Disposal of High Level and Long Lived Radioactive Waste in France*; Nuclear Energy Agency Organisation for Economic Co operation and Development, 2006.
(6) Hoth, P.; Wirth, H.; Reinhold, K.; Bräuer, V.; Krull, P.; Feldrappe, H. *Endlagerung radioaktiver Abfälle in tiefen geologischen Formationen Deutschlands—Untersuchung und Bewertung von Tonges teinsformationen*; BGR Bundesanstalt für Geowissenschaften und Rohstoffe: Hannover, Germany, 2007.
(7) *NAGRA Projekt Opalinuston—Synthese der geowissenschaftlichen Untersuchungsergebnisse, Entsorgungsnachweis für abgebrannte Brennele mente, verglaste hochaktive sowie langlebige mittelaktive Abfälle*; NAGRA Nationale Genossenschaft für die Lagerung radioaktiver Abfälle: Wettingen, Switzerland, 2002.
(8) Mengel, K.; Röhlig, K. J.; Geckeis, H. Endlagerung radioaktiver Abfälle. *Chem. Unserer Zeit* **2012**, *46*, 208−217.
(9) Röhlig, K. J.; Geckeis, H.; Mengel, K. Endlagerung radioaktiver Abfälle. *Chem. Unserer Zeit* **2012**, *46*, 140−149.
(10) Hansen, F. D.; Leigh, C. D. *Salt Disposal of Heat Generating Nuclear Waste*; Sandia National Laboratories: Albuquerque, NM, 2011.
(11) Gaucher, E.; Robelin, C.; Matray, J. M.; Négrel, G.; Gros, Y.; Heitz, J. F.; Vinsot, A.; Rebours, H.; Cassagnabère, A.; Bouchet, A. ANDRA underground research laboratory: interpretation of the mineralogical and geochemical data acquired in the Callovian Oxfordian formation by investigative drilling. *Phys. Chem. Earth* **2004**, *29*, 55−77.
(12) Allen, T. R.; Stoller, R. E.; Yamanaka, S. *Comprehensive Nuclear Materials*; Elsevier: Amsterdam, The Netherlands, 2012. Radarweg 29, PO Box 211, 1000 AE.
(13) Courdouan, A.; Christl, I.; Meylan, S.; Wersin, P.; Kretzschmar, R. Isolation and characterization of dissolved organic matter from the Callovo Oxfordian formation. *Appl. Geochem.* **2007**, *22*, 1537−1548.
(14) Courdouan, A.; Christl, I.; Meylan, S.; Wersin, P.; Kretzschmar, R. Characterization of dissolved organic matter in anoxic rock extracts and in situ pore water of the Opalinus Clay. *Appl. Geochem.* **2007**, *22*, 2926−2939.
(15) Thurman, E. M. *Organic Geochemistry of Natural Waters*; Springer: Dordrecht, 1985.
(16) Wood, S. A. The aqueous geochemistry of the rare earth elements: Critical stability constants for complexes with simple carboxylic acids at 25°C and 1 bar and their application to nuclear waste management. *Eng. Geol.* **1993**, *34*, 229−259.
(17) Hummel, W.; Anderegg, G.; Rao, L.; Puigdomenech, I.; Tochiyama, O. *Chemical Thermodynamics of Compounds and Complexes of U, Np, Pu, Am, Tc, Se, Ni and Zr with Selected Organic Ligands*; Elsvier, 2005.
(18) Schnitzer, M.; Khan, S. U. *Humic Substances in the Environment*; M. Dekker, 1972.
(19) Geckeis, H.; Lützenkirchen, J.; Polly, R.; Rabung, T.; Schmidt, M. Mineral water interface reactions of actinides. *Chem. Rev.* **2013**, *113*, 1016−1062.
(20) Choppin, G. R. The role of natural organics in radionuclide migration in natural aquifer systems. *Radiochim. Acta* **1992**, *58*−*59*, 113−120.
(21) Hakanen, M.; Ervanne, H. *The Influence of Organic Cement Additives on Radionuclide Mobility A Literature Survey*, Finland, 2006; p 42.
(22) Greenfield, B. F.; Ilett, D. J.; Ito, M.; McCrohon, R.; Heath, T. G.; Tweed, C. J.; Williams, S. J.; Yui, M. The Effect of Cement Additives on Radionuclide Solubilities. *Radiochim. Acta* **1998**, *82*, 27−32.
(23) Skerencak Frech, A.; Maiwald, M.; Trumm, M.; Froehlich, D. R.; Panak, P. J. The complexation of Cm(III) with oxalate in aqueous solution at T = 20 90 degrees C: a combined TRLFS and quantum chemical study. *Inorg. Chem.* **2015**, *54*, 1860−1868.
(24) Skerencak Frech, A.; Trumm, M.; Fröhlich, D. R.; Panak, P. J. Coordination and Thermodynamics of Trivalent Curium with Malonate at Increased Temperatures: A Spectroscopic and Quantum Chemical Study. *Inorg. Chem.* **2017**, *56*, 10172−10180.
(25) Fröhlich, D. R.; Trumm, M.; Skerencak Frech, A.; Panak, P. J. The Complexation of Cm(III) with Succinate Studied by Time Resolved Laser Fluorescence Spectroscopy and Quantum Chemical Calculations. *Inorg. Chem.* **2016**, *55*, 4504−4511.
(26) Fröhlich, D. R.; Koke, C.; Maiwald, M. M.; Chomyn, C.; Plank, J.; Panak, P. J. A spectroscopic study of the complexation reaction of trivalent lanthanides with a synthetic acrylate based PCE super plasticizer. *Spectrochim. Acta, Part A* **2019**, *207*, 270−275.
(27) Fröhlich, D. R.; Maiwald, M. M.; Taube, F.; Plank, J.; Panak, P. J. A thermodynamical and structural study on the complexation of trivalent lanthanides with a polycarboxylate based concrete super plasticizer. *Dalton Trans.* **2017**, *46*, 4093−4100.
(28) Fellhauer, D.; Rothe, J.; Altmaier, M.; Neck, V.; Runke, J.; Wiss, T.; Fanghänel, T. Np(V) solubility, speciation and solid phase formation in alkaline $CaCl_2$ solutions. Part I: Experimental results. *Radiochim. Acta* **2016**, *104*, 355−379.
(29) Müller, K.; Foerstendorf, H.; Tsushima, S.; Brendler, V.; Bernhard, G. Direct spectroscopic characterization of aqueous actinyl(VI) species: A comparative study of Np and U. *J. Phys. Chem. A* **2009**, *113*, 6626−6632.
(30) Müller, K.; Foerstendorf, H.; Brendler, V.; Bernhard, G. Sorption of Np(V) onto TiO_2, SiO_2, and ZnO: An in situ ATR FT IR spectroscopic study. *Environ. Sci. Technol.* **2009**, *43*, 7665−7670.
(31) Glasoe, P. K.; Long, F. A. Use of glass electrodes to measure acidities in deuterium oxide. *J. Phys. Chem.* **1960**, *64*, 188−190.
(32) Vasiliev, A. N.; Banik, N. L.; Marsac, R.; Froehlich, D. R.; Rothe, J.; Kalmykov, S. N.; Marquardt, C. M. Np(V) complexation with propionate in 0.5 4 M NaCl solutions at 20 85 degrees C. *Dalton Trans.* **2015**, *44*, 3837−3844.
(33) Altmaier, M.; Metz, V.; Neck, V.; Müller, R.; Fanghänel, T. Solid liquid equilibria of $Mg(OH)_2(cr)$ and $Mg_2(OH)_3Cl{\cdot}4H_2O(cr)$ in the system Mg Na H OH Cl H_2O at 25°C. *Geochim. Cosmochim. Acta* **2003**, *67*, 3595−3601.
(34) Denecke, A. M.; Rothe, J.; Dardenne, K.; Blank, H.; Hormes, J. The INE Beamline for Actinide Research at ANKA. *Phys. Scr.* **2005**, *T115*, 1001−1003.
(35) Rothe, J.; Butorin, S.; Dardenne, K.; Denecke, M. A.; Kienzler, B.; Löble, M.; Metz, V.; Seibert, A.; Steppert, M.; Vitova, T.; Walther, C.; Geckeis, H. The INE Beamline for actinide science at ANKA. *Rev. Sci. Instrum.* **2012**, *83*, 043105.
(36) Rothe, J.; Denecke, M. A.; Dardenne, K.; Fanghänel, T. The INE Beamline for actinide research at ANKA. *Radiochim. Acta* **2006**, *94*, 691−696.
(37) Scheinost, A. C.; Claussner, J.; Exner, J.; Feig, M.; Findeisen, S.; Hennig, C.; Kvashnina, K. O.; Naudet, D.; Prieur, D.; Rossberg, A.; Schmidt, M.; Qiu, C.; Colomp, P.; Cohen, C.; Dettona, E.; Dyadkin, V.; Stumpf, T. ROBL II at ESRF: a synchrotron toolbox for actinide research. *J. Synchrotron Radiat.* **2021**, *28*, 333−349.
(38) Matz, W.; Schell, N.; Bernhard, G.; Prokert, F.; Reich, T.; Claußner, J.; Oehme, W.; Schlenk, R.; Dienel, S.; Funke, H.; Eichhorn, F.; Betzl, M.; Pröhl, D.; Strauch, U.; Hüttig, G.; Krug, H.; Neumann, W.; Brendler, V.; Reichel, P.; Denecke, M. A.; Nitsche, H. ROBL a CRG beamline for radiochemistry and materials research at the ESRF. *J. Synchrotron Radiat.* **1999**, *6*, 1076−1085.
(39) George, G. N.; Pickering, I. J. *EXAFSPAK: A Suite of Computer Programs for Analysis of X Ray Absorption Spectra*; SSRL: Stanford, 1995.
(40) Newville, M. IFEFFIT:interactive XAFS analysis andFEFFfit ting. *J. Synchrotron Radiat.* **2001**, *8*, 322−324.
(41) Ravel, B.; Newville, M. ATHENA, ARTEMIS, HEPHAESTUS: data analysis for X ray absorption spectroscopy using IFEFFIT. *J. Synchrotron Radiat.* **2005**, *12*, 537−541.
(42) Ankudinov, A. L.; Ravel, B.; Rehr, J. J.; Conradson, S. D. Real space multiple scattering calculation and interpretation of x ray absorption near edge structure. *Phys. Rev. B: Condens. Matter Mater. Phys.* **1998**, *58*, 7565−7576.
(43) Rehr, J. J.; Kas, J. J.; Prange, M. P.; Sorini, A. P.; Takimoto, Y.; Vila, F. Ab initio theory and calculations of X ray spectra. *C. R. Phys.* **2009**, *10*, 548−559.

(44) Bombieri, G.; Benetollo, F.; Del Pra, A.; Rojas, R. Structural studies on the actinide carboxylates IV The crystal and molecular structure of succinate dioxouranium(VI) monohydrate. *J. Inorg. Nucl. Chem.* **1979**, *41*, 201−203.
(45) Rojas, R. M.; Del Pra, A.; Bombieri, G.; Benetollo, F. Structural studies on actinides carboxylates V[1]. *J. Inorg. Nucl. Chem.* **1979**, *41*, 541−545.
(46) Furche, F.; Ahlrichs, R.; Hättig, C.; Klopper, W.; Sierka, M.; Weigend, F. Turbomole. *Wiley Interdiscip. Rev.: Comput. Mol. Sci.* **2014**, *4*, 91−100.
(47) Becke, A. D. A new mixing of Hartree Fock and local density functional theories. *J. Chem. Phys.* **1993**, *98*, 1372−1377.
(48) Küchle, W.; Dolg, M.; Stoll, H.; Preuss, H. Energy adjusted pseudopotentials for the actinides. Parameter sets and test calculations for thorium and thorium monoxide. *J. Chem. Phys.* **1994**, *100*, 7535−7542.
(49) Weigend, F.; Häser, M. RI MP2: first derivatives and global consistency. *Theor. Chem. Acc.* **1997**, *97*, 331−340.
(50) Weigend, F.; Häser, M.; Patzelt, H.; Ahlrichs, R. RI MP2: optimized auxiliary basis sets and demonstration of efficiency. *Chem. Phys. Lett.* **1998**, *294*, 143−152.
(51) Klamt, A.; Schüürmann, G. COSMO: a new approach to dielectric screening in solvents with explicit expressions for the screening energy and its gradient. *J. Chem. Soc., Perkin Trans. 1* **1993**, *25*, 799−805.
(52) Neck, V.; Fanghänel, T.; Rudolph, G.; Kim, J. I. Thermodynamics of Neptunium(V) in Concentrated Salt Solutions: Chloride Complexation and Ion Interaction (Pitzer) Parameters for the NpO_2^+ Ion. *Radiochim. Acta* **1995**, *69*, 39−48.
(53) Maiwald, M. M.; Fellhauer, D.; Skerencak Frech, A.; Panak, P. J. The complexation of neptunium(V) with fluoride at elevated temperatures: Speciation and thermodynamics. *Appl. Geochem.* **2019**, *104*, 10−18.
(54) Maiwald, M. M.; Sittel, T.; Fellhauer, D.; Skerencak Frech, A.; Panak, P. J. Thermodynamics of neptunium(V) complexation with sulfate in aqueous solution. *J. Chem. Therm.* **2018**, *116*, 309−315.
(55) Hagan, P. G.; Cleveland, J. M. The absorption spectra of neptunium ions in perchloric acid solution. *J. Inorg. Nucl. Chem.* **1966**, *28*, 2905−2909.
(56) Maiwald, M. M.; Skerencak Frech, A.; Panak, P. J. The complexation and thermodynamics of neptunium(V) with acetate in aqueous solution. *New J. Chem.* **2018**, *42*, 7796−7802.
(57) Zhang, Z.; Yang, Y.; Liu, G.; Luo, S.; Rao, L. Effect of temperature on the thermodynamic and spectroscopic properties of Np(v) complexes with picolinate. *RSC Adv.* **2015**, *5*, 75483−75490.
(58) Yang, Y.; Zhang, Z.; Liu, G.; Luo, S.; Rao, L. Effect of temperature on the complexation of NpO_2^+ with benzoic acid: Spectrophotometric and calorimetric studies. *J. Chem. Therm.* **2015**, *80*, 73−78.
(59) Skerencak, A.; Panak, P. J.; Hauser, W.; Neck, V.; Klenze, R.; Lindqvist Reis, P.; Fanghanel, T. TRLFS study on the complexation of Cm(III) with nitrate in the temperature range from 5 to 200 degrees C. *Radiochim. Acta* **2009**, *97*, 385−393.
(60) Skerencak, A.; Panak, P. J.; Fanghänel, T. Complexation and thermodynamics of Cm(III) at high temperatures: the formation of $[Cm(SO_4)_n]^{3-2n}$ (n = 1, 2, 3) complexes at T = 25 to 200°C. *Dalton Trans.* **2013**, *42*, 542−549.
(61) Alderighi, L.; Gans, P.; Ienco, A.; Peters, D.; Sabatini, A.; Vacca, A. Hyperquad simulation and speciation (HySS): a utility program for the investigation of equilibria involving soluble and partially soluble species. *Coord. Chem. Rev.* **1999**, *184*, 311−318.
(62) Puigdomènech, I.; Rard, J. A.; Plyasunov, A. V.; Grenthe, I.; Seine st Germain, L.; Des Îles, B. *Temperature Corrections to Thermodynamic Data and Enthalpy Calculations*; Issy les Moulineaux, France, 1999. Le Seine St. Germain 12, Bd. des Îles, F 92130.
(63) Kettler, R. M.; Palmer, D. A.; Wesolowski, D. J. Dissociation quotients of succinic acid in aqueous sodium chloride media to 225° C. *J. Solution Chem.* **1995**, *24*, 65−87.
(64) Kettler, R. M.; Wesolowski, D. J.; Palmer, D. A. Dissociation quotients of malonic acid in aqueous sodium chloride media to 100 C. *J. Solution Chem.* **1992**, *21*, 883−900.
(65) Smith, R.; Martell, A.; Motekaitis, R. *NIST Standard Reference Database 46 Version 6*, 2004.
(66) Daniele, P. G.; Rigano, C.; Sammartano, S. The formation of proton and alkali metal complexes with ligands of biological interest in aqueous solution. Thermodynamics of H^+, Na^+ and K^+ oxalate complexes. *Thermochim. Acta* **1981**, *46*, 103−116.
(67) Daniele, P. G.; Rigano, C.; Sammartano, S. The formation of proton and alkali metal complexes with ligands of biological interest in aqueous solution. Thermodynamics of Li^+, Na^+ and K^+ dicarboxylate complex formation. *Thermochim. Acta* **1983**, *62*, 101−112.
(68) Hummel, W.; Puigdomènech, I.; Rao, L.; Tochiyama, O. Thermodynamic data of compounds and complexes of U, Np, Pu and Am with selected organic ligands. *C. R. Chim.* **2007**, *10*, 948−958.
(69) Martell, A.; Smith, R. M.; Motekaitis, R. J. *NIST Standard Reference Database 46 Version 8.0: NIST Critically Selected Stability Constants of Metal Complexes*; U.S. Department of Commerce,Tech nology Administration, National Institute of Standards and Technol ogy: Gaithersburg, MD, 2004. Standard Reference Data Program.
(70) Maiwald, M. M.; Trumm, M.; Dardenne, K.; Rothe, J.; Skerencak Frech, A.; Panak, P. J. Speciation, thermodynamics and structure of Np(V) oxalate in aqueous solution. *Dalton Trans.* **2020**, *49*, 13359−13371.
(71) Fröhlich, D. R.; Skerencak Frech, A.; Panak, P. J. A spectroscopic study on the formation of Cm(III) acetate complexes at elevated temperatures. *Dalton Trans.* **2014**, *43*, 3958−3965.
(72) Maiwald, M. M.; Dardenne, K.; Rothe, J.; Skerencak Frech, A.; Panak, P. J. Thermodynamics and Structure of Neptunium(V) Complexes with Formate. Spectroscopic and Theoretical Study. *Inorg. Chem.* **2020**, *59*, 6067−6077.
(73) Guillaumont, R.; Fanghänel, T.; Neck, V.; Fuger, J.; Palmer, D. A. *Update on the Chemical Thermodynamics of Uranium, Neptunium, Plutonium, Americium and Technetium*; Elsvier, 2003.
(74) Hug, S. J.; Bahnemann, D. Infrared spectra of oxalate, malonate and succinate adsorbed on the aqueous surface of rutile, anatase and lepidocrocite measured with in situ ATR FTIR. *J. Electron Spectrosc. Relat. Phenom.* **2006**, *150*, 208−219.
(75) Deacon, G.; Phillips, R. J. Relationships between the carbon oxygen stretching frequencies of carboxylato complexes and the type of carboxylate coordination. *Coord. Chem. Rev.* **1980**, *33*, 227−250.
(76) Jones, L. H.; Penneman, R. A. Infrared Spectra and Structure of Uranyl and Transuranium(V) and (VI) Ions in Aqueous Perchloric Acid Solution. *J. Chem. Phys.* **1953**, *21*, 542−544.
(77) Allen, P. G.; Bucher, J. J.; Shuh, D. K.; Edelstein, N. M.; Reich, T. Investigation of Aquo and Chloro Complexes of UO_2^{2+}, NpO_2^+, Np^{4+}, and Pu^{3+} by X ray Absorption Fine Structure Spectroscopy. *Inorg. Chem.* **1997**, *36*, 4676−4683.
(78) Takao, K.; Takao, S.; Scheinost, A. C.; Bernhard, G.; Hennig, C. Complex formation and molecular structure of neptunyl(VI) and (V) acetates. *Inorg. Chem.* **2009**, *48*, 8803−8810.